Taylor & Francis
Taylor & Francis Group

Synthesis and Reactivity in Inorganic, Metal-Organic, and Nano-Metal Chemistry

ISSN: 1553-3174 (Print) 1553-3182 (Online) Journal homepage: http://www.tandfonline.com/loi/lsrt20

Nickel(II) complex of 4-Amino-N-(2-pyrimidinyl)benzenesulfonamide: Synthesis, spectroscopic characterization, antimicrobial activity, crystal structure and Hirshfeld surface analysis

Sanjay M. Tailor & Urmila H. Patel

To cite this article: Sanjay M. Tailor & Urmila H. Patel (2016): Nickel(II) complex of 4-Amino-N-(2-pyrimidinyl)benzenesulfonamide: Synthesis, spectroscopic characterization, antimicrobial activity, crystal structure and Hirshfeld surface analysis, Synthesis and Reactivity in Inorganic, Metal-Organic, and Nano-Metal Chemistry, DOI: 10.1080/15533174.2016.1158186

To link to this article: http://dx.doi.org/10.1080/15533174.2016.1158186

Nickel(II) complex of 4-Amino-N-(2-pyrimidinyl)benzenesulfonamide: Synthesis, spectroscopic characterization, antimicrobial activity, crystal structure and Hirshfeld surface analysis

Sanjay M. Tailor* and Urmila H. Patel

Department of Physics, Sardar Patel University, Vallabh Vidyanagar - 388 120, Gujarat, India

*Corresponding author:E-mail: sanjay_tailor10@yahoo.com

Abstract

Nickel complex of 4-Amino-N-(2-pyrimidinyl)benzenesulfonamide (sulfadiazine) has been synthesized and characterized by elemental analysis, infrared, UV-Vis and ^{1}H NMR spectroscopy. The title compound, $[Ni(C_{10}H_9N_4O_2S)_2(C_5H_5N)_2](C_5H_5N)(H_2O)_2$ crystallizes in monoclinic system with space group $P2_1$ and Z=2. X-ray analysis revealed that Ni(II) ion exhibits a distorted octahedral geometry. The Hirshfeld surfaces are performed to study the nature of interactions and their quantitative contributions towards crystal packing. The results of spectral and thermal data suggest that binding of nickel atom to the sulfonamidic nitrogen are in agreement with the crystal structure determination. Nickel sulfadiazine presents different antibacterial behavior against *Escherichia coli* and *Staphylococcus aureus* strains.

Keywords

Ni complex; Spectroscopic analysis; Crystal structure; Hirshfeld surface; Thermogravimetric study; Antimicrobial activity

1. Introduction

Among the many different families of organic–inorganic chemicals being currently investigated due to their wide scale applications, sulfonamides and their N-derivatives are one of the outstanding groups [1]. Sulfadiazine is considered as a Sulfa-drug derived from the parent compound, sulfanilamide, which consider important class of drugs with several types of pharmacological agents possessing antibacterial [2], antithyroid [3], diuretic [4,5], hypoglycaemic [6], and anti-carbonic anhydrase [7,8]. The pharmacological activity of these types of molecules is often enhanced by complexation with metal ions [9,10]. Thus, rapid healing of skin disorders has been promoted by silver sulfadiazine complex [11,12] in human topical burn therapy, and zinc sulfadiazine complex [13,14] in the prevention of bacterial infection in burned animals, where the effectiveness of burn treatment seems to depend not only on the presence of a metal ion [slow release of the Ag(I) or Zn(II)], but also crucially on the nature of the material to which the metal ion is bound [13]. Sulfadiazine (sdz), a well-known antibiotic sulfonamide, widely used for their bactericidial action and X-ray structures of them have been reported [15,16]. Our interest is in the synthesis and characterization of metallic complexes bearing sulfonamide ligands. Since several sulfonamide metal complexes showed more activity than free ligand [17–19]. Sulfadiazine can act as a monodentate or a bidentate ligand containing several groups with donor atoms those are able to interact with metal ions: Ar–NH_2, NH sulfonamide, SO_2–R and N heterocyclic atoms (Figure 1).

Recently, the prediction and computation of molecular crystal structures through the aspect of intermolecular interactions, structural elucidation, crystal design and crystal engineering, also have aroused much attention [20–22]. The main approach is through Hirshfeld surfaces, which

serves as a powerful tool for elucidating molecular crystal structures [23]. Hirshfeld surfaces are space partitioning construct that summarizes the crystal packing into a single 3-D surface, and the surface can be reduced to a 2-D fingerprint plot, which summarizes the complex information on intermolecular interactions present in molecular crystals [22].

The crystal structures of $[Cu(sdz)_2(NH_3)_2]$ and $[Hg(sdz)_2(DMSO)_2]$ are reported by Brown et al. [24] and Garcia-Raso et al. [25], respectively. Additionally, Menabue et al. [26] reported the cadmium complex of sulfadiazine $[Cd(sdz)_2].2H_20$ having distorted tetrahedral geometry. Along with this, single crystal X-ray structure of $[Ni(C_{10}H_9N_4O_2S)_2(C_5H_5N)_2]\cdot 0.5H_2O$ is reported by Wang et al. [27].

In the present study, synthesis, spectroscopic characterization and antibacterial assays over gram positive and gram negative pathogenic bacterial strains of Ni(II) complex with sulfadiazine are described. A new crystal structure for the nickel sulfadiazine complex along with the influence of nickel metal on the ligand in terms of intermolecular interactions by using Hirshfeld surfaces and fingerprint plots are also reported here.

2. Experimental

2.1. Materials and methods

Sodium sulfadiazine (Sigma, >99%), nickel acetate and all other reagents are of the highest grade commercially available and used without further purification.

2.2. Physical measurements

Elemental analysis (C, H, N) is carried out using a Perkin Elmer 2400-II CHN elemental analyzer. IR spectra are recorded on a Perkin Elmer Spectrum GX FT-IR Spectrometer using KBr pellet. UV-Vis spectra (200-800 nm) are recorded on a Shimadzu UV-3600 spectrometer in

DMSO. ^{1}H NMR spectra are recorded on a Bruker Avance DPX-200 spectrometer in d^{6}-DMSO. Electrical conductivity is measured using EQ-660A conductivity meter. Thermogravimetric analysis is carried out at heating rate of 5°C min^{-1} in the temperature range of 25–967°C under nitrogen flow of 100 mL min^{-1} by a simultaneous TGA/DTA analyzer using Seiko SII-EXSTAR TG/DTA-7200.

2.3. Synthesis of the complex

Sodium salt of sulfadiazine (0.545 g, 2 mmol) is dissolved in hot methanol and to this, an aqueous solution of nickel acetate (0.176 g, 1 mmol) is added with constant stirring and the mixture is refluxed for 3 hours. A light blue precipitate is formed, filtered and washed with hot distilled water and methanol successively and dried in a desiccator over anhydrous $CaCl_2$. The yield at the end of reaction for the complex is around 35%. The results for $[C_{20}H_{22}N_8Ni_1O_6S_2]$ are: Anal. Calcd. (%): C, 40.49; H, 3.73; N, 18.88. Found (%): C, 40.16; H, 3.47; N, 17.54.

The complex is insoluble in water and in most of the common solvents but soluble in Dimethyl sulfoxide (DMSO), Dimethylformamide (DMF) and pyridine. A very few numbers of tiny light blue single crystals are grown from pyridine solvent adequate for X-ray structure analysis.

2.4. X-ray crystallography

Crystallographic data are collected on a Bruker Kappa APEX-II CCD diffractometer with graphite monochromated MoKα radiation (λ= 0.71703 Å) at T = 296.15 K. The X-ray diffraction data are corrected for Lorentz-polarization factor and scaled for absorption effects by evaluation of multi-scans. The structure is solved by direct methods with SHELXS-2013 [28] and anisotropic thermal parameters for all non hydrogen atoms are refined by full-matrix least squares procedure against F^2 with SHELXL-2013 [29]. The H atoms are positioned

geometrically with N–H=0.90Å for NH_2 and C–H=0.93Å for aromatic H atoms respectively. In addition they are constrained to ride on their parent atoms with $U_{iso}(H)=1.2\ U_{eq}$ (carrier atoms of CH, NH). The calculations concerning the molecular geometry, the choice and verification of the space group, the analysis of hydrogen bonds and C–H···π interactions are performed by PLATON [30]. The molecular graphics are done with ORTEP-3 [31] and WinGX [32].

2.5. Hirshfeld surface calculations

Molecular Hirshfeld surfaces [33] in the crystal structure have been constructed based on the electron distribution calculated as the sum of spherical atom electron densities [34]. For a given crystal structure and set of spherical atomic electron densities, the Hirshfeld surface is unique [35] suggesting the possibility of gaining additional imminent into the intermolecular interaction of molecular crystals. Hirshfeld surfaces and the associated 2-D fingerprint plots are generated using the Crystal Explorer 3.1 [36]. When the CIF file is read into the Crystal Explorer program for analysis, all bond lengths to hydrogen are automatically modified to typical standard neutron values (C–H = 1.083 Å and N–H = 1.009 Å). The 2-D fingerprint plots displayed by using the standard 0.6–2.8 Å view with the d_e and d_i distance scales displayed on the graph axes. The normalized contact distance (d_{norm}) based on both d_e, d_i and the *vdw* radii of the atom, given by Eq. (1) enables identification of the regions of particular importance to intermolecular interactions [33]. Because of the symmetry between d_e and d_i in the expression for d_{norm} , where two Hirshfeld surfaces touch, both will display a red spot identical in color intensity as well as size and shape.

$$d_{norm} = \left(d_i - r_i^{vdw}\right)/r_i^{vdw} + \left(d_e - r_e^{vdw}\right)/r_e^{vdw} \quad (1)$$

2.6. Microbiological assays

Micro broth dilution method is used to determine the minimal inhibitory concentration (MIC) of the antimicrobial agent against gram negative (*Escherichia coli*) and gram positive (*Staphylococcus aureus*). The steps for performing the Micro broth dilution method are based on recommendations from the National Committee for Clinical Laboratory Standards [37].

The standard strains used are *Escherichia coli* MTCC 422 and *Staphylococcus aureus* MTCC 96. Mueller Hinton Broth is used as Nutrient medium at 37˚C to grow and dilute the drug suspension for the test bacteria. The solvent DMSO is used as diluent to get desired concentration of drugs to test upon standard bacterial strains. Serial dilutions are prepared in primary and secondary screening. Each synthesized compound and standard drugs are diluted obtaining 2000 μg/mL concentration, as a stock solution. In primary screening 1000, 500, and 250 μg/mL concentrations of the synthesized drugs are taken. The active synthesized compounds found in this primary screening are further diluted to obtain 200, 125, 100, 62.5, 50, 25, 12.5, and 6.250 μg/mL concentrations for secondary screening. Inoculum's size for test strain is adjusted to 10^8 $CFU.ml^{-1}$ by comparing the turbidity. MIC is the lowest concentration of a compound in DMSO that exhibited no visual growth of the organisms in the culture tubes. Each of the above experiments is repeated thrice along with a control set using DMSO. The mean value obtained for three individual replicates is then used to calculate the growth inhibition zone of each sample.

3. Results and discussion

3.1. Crystal structure of $[Ni(C_{10}H_9N_4O_2S)_2(C_5H_5N)_2](C_5H_5N)(H_2O)_2$

Suitable single crystals grown by slow evaporation from a pyridine solvent of the complex is used for X-ray crystal structure determination. The single crystal data and refinement details for

the title compound, $[Ni(C_{10}H_9N_4O_2S)_2(C_5H_5N)_2](C_5H_5N)(H_2O)_2$ are summarized in Table 1. The fractional atomic coordinates and equivalent isotropic thermal parameters are tabulated in Table 2. Figure 2 shows an ORTEP view of the title compound with thermal displacement ellipsoids are drawn at 50% probability level.

The title compound, $[Ni(C_{10}H_9N_4O_2S)_2(C_5H_5N)_2](C_5H_5N)(H_2O)_2$ crystallizes in monoclinic crystal system with space group $P2_1$ and Z=2. Crystal structure of the title compound contains six coordinated nickel atom leading to a distorted octahedral geometry by two sulfonamidic nitrogen atoms, two pyrimidine nitrogen atoms (each from two sulfadiazine ligands) and two nitrogen atoms from two pyridine solvent molecules. In addition, the two water molecules and one pyridine molecule are as solvent which fill in the 3-D packing architecture, participate in the formation of an intricate 3-D network through hydrogen bond interactions. The distance between nickel cation and the nitrogen atoms adjacent to the sulfonyl group of a symmetry related ligand are Ni−N1 (2.128(4) Å for molecule A and 2.126(4) Å for molecule B) which is similar to the other reported Ni−N(sulfonamidic) distances [27,38,39]. Third and fourth bond involves the pyrimidine nitrogen atoms Ni−N2 (2.093(4) Å for molecule A and 2.094(4) Å for molecule B). The reported Ni−N(pyrimidine) distances for $[Ni(C_{10}H_9N_4O_2S)_2(C_5H_5N)_2]\cdot 0.5H_2O$ [27] and $[Ni(smr)_2(pyr)_2]\cdot 4pyr$ [38] are 2.070(2) and 2.100(2), respectively. Fifth and sixth bond occurs with the pyridine nitrogen atoms Ni−N5 (2.097(3) Å for molecule A and 2.102(3) Å for molecule B) which is similar Ni−N(pyridine) distance 2.100(3) Å reported in $Ni(smtz)_2(py)_2(OH_2)_2$ [40], but quite shorter than reported (2.134(2) and 2.159(2) Å) in nickel sulfadiazine complex [27].

The selected bond lengths and bond angles are tabulated in Table 3. The bond lengths and angles of the phenyl ring confirm well to those found in the free sulfadiazine [15,16], whereas distances S1–N1 (1.599(4) Å for molecule A and 1.590(4) Å for molecule B) and N1–C7 (1.369(6) Å for molecule A and 1.369(6) Å for molecule B) are shorter in the Ni(II) complex than those found in free sulfadiazine ligand [15,16]. The stereochemistry about the sulfur atom is as usual a slightly distorted tetrahedral geometry with the bond lengths and bond angles involving sulfur lying within the range quoted in the literature [41–43]. The maximum and minimum value of angles around the sulfur atom are O1–S1–O2 (117.6(3)˚ for molecule A and 116.6(2)˚ for molecule B) and O2–S1–N1 (104.3(2)˚ for molecule A and 111.7(2)˚ for molecule B) and the S–N bond length is similar to that found in $[Ni(C_{10}H_9N_4O_2S)_2(C_5H_5N)_2]\cdot 0.5H_2O$ [27]. The *gauche* conformation bout the S–N(sulfonamidic) bond with a torsion angle of 74.4(4)˚ for molecule A and -74.1(3)˚ for molecule B, but the angle is higher (-53.9˚) in silver sulfadiazine [11]. The reported *gauche* conformation about the S–N(sulfonamidic) bond for free sulfadiazine molecule with torsion angle 77˚ [15]. The dihedral angle between phenyl and pyrimidine ring for title compound are 67.1(2)˚ for molecule A and 69.6(2)˚ for molecule B, while in free sulfadiazine molecule the angle is 76˚ [15].

In the crystal structure, the molecular stability is due to strong intermolecular and intramolecular interactions. Out of all these, three of the intermolecular interactions are N–H···O hydrogen bond formed by the terminal amino nitrogen and water molecule oxygen and two O–H···O hydrogen bonds formed between the water molecule oxygen and sulfonyl oxygen. The packing diagram of the title compound, $[Ni(C_{10}H_9N_4O_2S)_2(C_5H_5N)_2](C_5H_5N)(H_2O)_2$ with N–H···O, O−H···O and C−H···O intermolecular interactions are shown in Figure 3. In the title compound, amino

nitrogen atom acts as an acceptor forming intermolecular C–H···N and O–H···N hydrogen bond interactions. Water molecules play a significant role in the crystal packing acting as a donor/acceptor. The packing diagram of the title compound with C−H···N and O–H···N intermolecular interactions are depicted in Figure 4. The intramolecualar C–H···O interaction is formed between phenyl ring carbon of sulfadiazine and the sulfonyl oxygen atom. The crystal structure is also exhibits C(14A)–H(14A)···Cg(8) interaction [where Cg(8) is the centroid of the ring C1B/C2B/C3B/C4B/C5B/C6B with a symmetry code 1+x, y, z] with a C–Cg distance of 3.605(7) Å, C–H···Cg angle of 172˚. Hydrogen bond geometry and symmetry code for title compound are summarized in Table 4.

3.2. Hirshfeld surface analysis

The Hirshfeld surfaces and consequently the fingerprint analysis have been performed to study the nature of interactions and their quantitative contributions towards the crystal packing. The molecular Hirshfeld surfaces of title compound, $[Ni(C_{10}H_9N_4O_2S)_2(C_5H_5N)_2](C_5H_5N)(H_2O)_2$ generated using a standard (high) surface resolution with the 3-D d_{norm} surfaces are mapped over a fixed color scale of -0.65 (red) to 1.3 Å (blue), d_i and d_e surfaces are mapped in the range of 0.7–2.7, shape index mapped in the color range of -1.0–1 and curvedness in the range of -4.0–0.4 (Figure 5). For each point on the iso-surface two different types of distances are defined: one is d_e signifying the distance from the point to the nearest nucleus external to the surface and the other one is d_i signifying the distance to the nearest nucleus internal to the surface. The normalized contact distance (d_{norm}) is based on both d_e and d_i. The surfaces are displayed as transparent to permit visualization of the title compound, around which they are calculated. The surface represented with a spherical depression (deep red) spot is indicative of hydrogen bonding

interactions (Figure 5a). The dominant interactions are H···O (Figure 5b), can be seen in d_i surface plots as the bright red color spots. The deep red color spots in d_e (Figure 5c) are strong interactions such as O···H (14.7%). The shape index is a measure of ‘‘which shape’’, and it can be sensitive to very subtle changes in surface shape, particularly in areas where the total curvature (or the curvedness) is very low (Figure 5d). The curvedness surface (Figure 5e) is the measurement of ‘‘how much shape’’; the flat areas of the surface correspond to low values of curvedness, while sharp curvature areas correspond to high values of curvedness. The small range of region and light color on the surface symbolize a weaker and longer interaction other than hydrogen bonds. The 2-D fingerprint plots of title compound exemplify the strong indication for the all intermolecular interaction at the same time (Figure 6a). The H—H contacts, which are reflected in the middle of scattered points and cover most area in the 2-D fingerprint plots, have a most significant contribution to the total Hirshfeld surfaces (46.8%) (Figure 6b). At the top left and bottom right of the fingerprint plot, there are characteristic ‘‘wings’’ which are identified as a result of C—H contacts (Figure 6c). The decomposition of the fingerprint plot shows that C—H/H—C contacts comprise 27.3% of the total Hirshfeld surface area. In the fingerprint region (Figure 6d), H···O (14.7%) interactions are represented by a spike in the top area whereas the O···H (14.7%) interactions are represented by a spike in the lower part of fingerprint plot. Similar behaviour is observed for the corresponding C–H···N intermolecular interaction. A greater value of d_i is indicating the presence of the amino group where the N4 atom is acting as a good acceptor (Figure 6e). The proportion of N—H/H—N contacts comprising 8.3% of the total Hirshfeld surfaces. The C—C contact on the fingerprint plot (Figure 6f) is presented as characteristic stacking kite, which is mainly assigned to π-π interaction. This

is reflected by red–blue triangles on the shape index surface of the title compound (Figure 5d). The C—C contact includes only 2.8% of the Hirshfeld surfaces with equal *d*i =*d*e. The 2-D fingerprint plot (Figure 6g) for C—N/N—C contacts comprise 0.1% of the total Hirshfeld surface area. Hydrogen bonding interactions H···H (46.8%) are very high compared to the other bonding interactions. The quantitative interactions with percentages are analyzed and displayed in pie chart (Figure 7).

3.3. IR spectra

The infrared spectra (IR) of the complex taken in the region 4000-400 cm^{-1} are compared with the free sulfadiazine ligand. Based on some general references [44–46] and previous studies of complexes with sulfonamides [47–49], the positions of the characteristic vibrations of the free sulfadiazine and its nickel complex is tabulated in Table 5.

The bands appear between 3450 and 3360 cm^{-1} are due to asym(NH_2) and sym(NH_2) vibrations of the amino (–NH_2) group are modified with respect to the free sulfadiazine ligand. These modifications are most probably due to the hydrogen bonding between complexes involving the NH_2 and SO_2 groups.

The peak for the sulfonamidic (N–H) group in the free ligand at around 3102 cm^{-1}, is absent in the spectra of the complex, confirming the deprotonation of the –SO_2NH– moiety. The scissoring vibration of nickel sulfadiazine complex for the amino (–NH_2) group observed at 1628 cm^{-1} and peaks due to phenyl ring appear at around 1558 and 1595 cm^{-1}. The peaks around 1267 and 1360 cm^{-1} are assigned to $\nu_{as}(SO_2)$, and those at 1183 cm^{-1} to $\nu_{sy}(SO_2)$, show significant changes upon complexation.

The band in the free sulfadiazine ligand at 942 cm^{-1} assigned to ν(S–N) [18, 25]. The bands at higher frequencies (989 and 1015 cm^{-1}) in the complex are consequence of coordination to the metal. This shift to higher frequency is in accordance with the shortening of the S–N bond lengths, which has been observed in the crystal structure of complex. The bands of the ligand at 3424, 1651 and 942 cm^{-1} shifted to 3450, 1628 and 989 cm^{-1}, respectively, after coordination. Most of the other shifts are small.

3.4. ^{1}H NMR spectra

^{1}H NMR spectra of the free sulfadiazine and its nickel(II) complex are recorded in d^{6}-DMSO. The chemical shifts are expressed in ppm relative to internal TMS. The spectral data along with the possible assignments are presented in Table 6. All the protons due to heteroaromatic/aromatic groups are found as to be in their expected region [50]. From the data, it is reflected that the ligand present in the complex exhibits very small shifts in comparison to the free ligand. The conclusion drawn from these studies, the proton magnetic resonance spectrum of sulfadiazine shows a broad singlet at 11.259 ppm, which may be assigned to the sulfonamide NH proton. The absence of this proton signal in the spectra of the nickel sulfadiazine complex indicate that the sulfonamide NH group is deprotonated during complex formation.

3.5. UV-Vis spectra

The UV spectra of free sulfadiazine and its nickel complex recorded in DMSO solution are depicted in Figure 8. The electronic spectrum of sulfadiazine gave absorption band at 275 nm assigned to π→π*. The electronic spectra of the nickel sulfadiazine complex similarly show the transitions which are slightly shifted to shorter wavelengths (272 nm) as a result of decrease in conjugation of the system after complexation. Nickel sulfadiazine complex presented two bands

in the visible region. The splitting of one of them is due to spin–orbit coupling that mixed the $^3T_{1g}(F)$ and ^1E_g states [51]. The absorbance bands for Ni-sdz found in the range 398-405 nm due to $^3A_{2g} \rightarrow {}^3T_1g(F)$ and 600-650 nm attributed to $^3A_{2g} \rightarrow {}^1E_g$ which is assigned to d-d transitions of a distorted octahedral Ni(II) chromophore. The absorbance value of sulfadiazine (sdz) and its nickel complex are listed in Table 7.

3.6. Thermogravimetric analysis

Sulfadiazine (sdz) and its nickel complex (Ni-sdz) are studied by thermogravimetric analysis from ambient temperature to 967°C in nitrogen atmosphere. The TGA curves are shown as % mass loss versus temperature, the DTG curves are as the rate of loss of mass versus temperature. The compound decomposes mainly into three stages on heating between the room temperature and 967˚C. The decomposition pattern reveals that the first weight loss is 9.0% in the range of 43˚C–330˚C, which is ascribed to the loss of water molecules (calculated 10.0%), the second weight loss is 36.0% in the range of 330˚C–430˚C, which is due to the loss of aniline moiety and oxygen atoms (calculated 36.8%). With further heating, the 30.0% of the compound (calculated 31.7%) decomposed between 420˚C and 967˚C, which is ascribed to the loss of pyrimidine moiety and sulfur atom. The differences between the experimental and calculated weight losses in three stages of decomposition are negligible and are within the experimental errors. Above 967˚C, 25% of the residue are left out which is attributed to the charring of nickel salt. Hence, the TG study confirms the formation of the compound in the stoichiometric ratio.

The thermal decomposition of nickel complex of sulfadiazine occurs with DTG curve maxima showing endothermic peak at 70.80°C (ΔH = 34.84 kJmol^{-1}) and 398.40°C (ΔH =115.89 kJmol^{-1}) while in free sulfadiazine endothermic peak are observed at 275.80°C (ΔH = 144.287 kJmol^{-1})

and 339.80°C (ΔH = 23.333 $kJmol^{-1}$). The final residual mass left at 967°C correspond to 25.29% for nickel complex and 25.60% for free sulfadiazine. The thermogravimetric (TG) and differential thermogravimetric (DTG) curves for free sulfadiazine and its nickel complex are depicted in Figure 9 and 10. Thermodynamic parameters of the synthesized nickel complex of sulfadiazine and ligand (sdz) itself have been evaluated by Broido's graphical method [52] for straight line decomposition portion of the thermodynamic analytical curve. Activation Energy (E_a) is calculated by the slope of ln(ln1/y) versus 1/T, where y is the fraction of the number of initial molecules not yet decomposed. The thermodynamic parameters like change in enthalpy (ΔH), entropy (ΔS), Gibb's free energy (ΔG) and Arrhenius constant (A) are calculated using the standard equations [53,54] and data are presented in Table 8.

3.7. Electrical conductivity measurement

The electrical conductivity of sulfadiazine and its nickel complex in 10^{-3} M pyridine solution are measured at room temperature. The molar conductance (Λ_m) values of sulfadiazine and its nickel complex are 6.02 and 5.49 ohm^{-1} cm^2 mol^{-1}, respectively showing their non-electrolytic [55] nature. The results indicate that no anion is present outside the coordination sphere. The very low molar conductivity value of nickel sulfadiazine complex reveals that complex remain neutral in solution.

3.8. Microbiological assays

The minimum inhibitory concentration (MIC) values of sulfadiazine and its nickel complex against *Staphylococcus aureus* and *Escherichia coli* are shown in Table 9. Sulfadiazine and its nickel complex exhibited varying inhibitory effect toward the bacterial strains. The complex has ability to kill the investigated bacteria with large inhibition zone diameters comparing with that

of free ligand, but at higher concentration than the sodium salt. Sulfonamides penetrate bacterial cells in the neutral form, and once inside a cell, their bacterial action is from the ionized form [56]. The nickel sulfadiazine complex is sensitive toward gram negative bacteria (*Escherichia coli*) while it is not active against gram positive bacteria (*Staphylococcus aureus*).

Our observations reveal that the MIC for nickel complex changes according to the target bacteria. It is known that *Staphylococcus aureus* and *Escherichia coli* have different cell wall constitution. *Escherichia coli* has an outer lipidic membrane layer while *Staphylococcus aureus* does not have one.

4. Conclusion

Nickel complex of sulfadiazine is synthesized, characterized and tested as antimicrobial agents. Single crystals of nickel sulfadiazine complex are successfully grown from pyridine solution by using slow evaporation technique. The molecular structure of title compound is determined by single crystal XRD and which reveals that the Ni(II) ion exhibit a distorted octahedral geometry. Hirshfeld surfaces are employed to confirm the existence of intermolecular interactions in the title compound. The spectroscopic data are in good agreement with the crystal structure. Ni-sdz shows higher antibacterial activity than free ligand against gram negative bacteria (*Escherichia coli*).

Supplementary data

Full crystallographic data for the structure reported in this article have been deposited in the Cambridge Crystallographic Data Center, CCDC No. 1008229. Copies of this information can be obtained, free of charge, on application to CCDC, 12 Union Road, Cambridge, CB2 1EZ, U.K. (Fax: +44-1223-336033; or E-mail: deposit@ccdc.cam.ac.uk).

Acknowledgement

We are thankful to DST- FIST, New Delhi for funding towards the single crystal diffractometer facility at Department of Physics, Sardar Patel University, Vallabh Vidyanagar. One of the authors (SMT) is thankful to UGC for RFSMS fellowship. We are also thankful to Central Salt and Marine Chemicals Research Institute, CSMCRI, Bhavnagar for collecting NMR and TGA data. We also acknowledge the help received from SICART, Vallabh Vidyanagar for CHN and IR data.

References

[1] Blasco, F.; Perello´, L.; Latorre, J.; Borra´s, J.; Garcia´-Granda, S. *J. Inorg. Biochem.* **1996**, 61, 143.

[2] Drews, J. *Science* **2000**, 287, 1960.

[3] Thornber, C.W. *Chem. Soc. Rev.* **1979**, 8, 563.

[4] Supuran, C.T. *Nat. Rev. Drug Discov.* **2008**, 7, 168.

[5] Maren, T.H. *Annu. Rev. Pharmacol. Toxicol* **1976**, 16, 309.

[6] Boyd, A.E. *Diabetes* **1988**, 37, 847.

[7] Supuran, C.T.; Scozzafava, A. *Exp. Opin. Ther. Patents* **2000**, 10, 575.

[8] El-Henawy, A.A.; Mohamed, S.I.; Hassan, A.A.; Halawa, A.H.; Elnassag, M.A.; Elhage, G. A. *New York Science Journal* **2011**, 4, 19.

[9] Bult, A. *Metal Ions in Biological Systems*, Vol. 16, Sigel, H., (Eds.), Marcel Dekker, New York, **1983**.

[10] Casanova, J.; Alzuet, G.; Ferrer, S.; Borra´s, J.; Garc´ıa-Granda, S.; Perez-Carren˜o, E. *J. Inorg. Biochem.* **1993**, 51, 689.

[11] Baenziger, N.C.; Struss, A.W. *Inorg. Chem.* **1976**, 15, 1807.

[12] Cook, D.S.; Turner, M.F. *J. Chem. Soc., Perkin Trans. 2* **1975**, 1021.

[13] Baenziger, N.C.; Modak, S.L.; Fox, C.L. *Acta Crystallogr.* **1983**, C39, 1620.

[14] Brown, C.J.; Cook, D.S.; Sengier, L. *Acta Crystallogr.* **1987**, C43, 2332.

[15] Shin, H.S.; Ihn, G.S.; Kim, H.S.; Koo, C.H. *J. Korean Chem. Soc.* **1974**, 18, 329.

[16] Ajibade, P.A.; Kolawole, G.A.; Brien, P.O.; Helliwell, M.; Raftery, J. *Inorg. Chim. Acta.* **2006**, 359, 3111.

[17] Kremer, E.; Facchin, G.; Estevez, E.; Albores, P.; Baran, E.J.; Ellena, J.; Torre, M.H. *J. Inorg. Biochem.* **2006**, 100, 1167.

[18] Casanova, J.; Alzuet, G.; Borras, J.; Timoneda, J.; Garcıa-Granda, S.; Candano-Gonzalez, I. *J. Inorg. Biochem.* **1994**, 56, 65.

[19] Chohan, Z.H.; Mahmood-Ul-Hassan, K.; Khan, M.; Supuran, C.T. *J. Enzyme Inhib. Med. Chem.* **2005**, 20, 183.

[20] McKinnon, J.J.; Jayatilaka, D.; Spackman, M.A. *Chem. Commun.* **2007**, 3814.

[21] Tailor, S.M.; Patel, U.H. *Acta Cryst.* **2015**, C71, 944.

[22] Luo, Y.H.; Zhang, C.G.; Xu, B.; Sun, B.W. *Cryst. Eng. Commun.* **2012**, 14, 6860.

[23] Rigaku. *CrystalClear*, Version 14.0. Rigaku Corporation, Tokyo, Japan, **2005**.

[24] Brown, C.J.; Cook, D.S.; Sengier, L. *Acta Cryst.* **1985**, C41, 718.

[25] Garcia-Raso, A.; Fiol, J.J.; Martorell, G.; Lopez-Zafra, A.; Quiros, M. *Polyhedron* **1997**, 16, 613.

[26] Menabue, L.; Saladini, M. *J. Inorg. Biochem.* **1993**, 49, 201.

[27] Wang, Y.-F.; Li, F.-X.; Peng, Y.; Chen, Z.-F.; Liang, H. *Acta Cryst.* **2009**, E65, m1584.

[28] Sheldrick, G.M. *SHELXS2013: Program for Crystal Structure Solution*, University of Göttingen, Germany, **2013**.

[29] Sheldrick, G.M. *SHELXL2013: Program for Crystal Structure Refinement*, University of Göttingen, Germany, **2013**.

[30] Spek, A.L. *PLATON: A Multipurpose Crystallographic Tool*, Utrecht University, The Netherlands, **2003**.

[31] Farrugia, L.J. *J. Appl. Cryst.* **1997**, 30, 565.

[32] Farrugia, L.J. *J. Appl. Cryst.* **1999**, 32, 837.

[33] Spackman, M.A.; McKinnon, J.J. *Cryst. Eng. Comm.* **2002**, 4, 378.

[34] Spackman, M.A.; Byrom, P.G. *Chem. Phys. Lett.* **1997**, 267, 215.

[35] McKinnon, J.J.; Spackman, M.A.; Mitchell, A.S. *Acta Cryst.* **2004**, B60, 627.

[36] Wolff, S.K.; Grimwood, D.J.; McKinnon, J.J.; Turner, M.J.; Jayatilaka, D.; Spackman, M.A. *Crystal Explorer*, Version 3.1, University of Western Australia, **2012**.

[37] National Committee for Clinical Laboratory Standards. *Methods for Dilution Antimicrobial Susceptibility Tests for Bacteria that grow aerobically*, approved standard (M7A5), fifth ed., National Committee for Clinical Laboratory Standards: Wayne, PA, **2000**.

[38] Mondelli, M.; Brune´, V.; Borthagaray, G.; Ellena, J.; Nascimento, O.R.; Leite, C.Q.; Batista, A.A.; Torre, M.H. *J. Inorg. Biochem.* **2008**, 102, 285.

[39] Golzar Hossain, G.M.; Amoroso, A.J. *Acta Cryst.* **2006**, E62, m2721.

[40] Borra´s, E.; Alzuet, G.; Borra´s, J.; Server-Carrio´, J.; Castin˜ eiras, A.; Liu-Gonza´lez, M.; Sanz-Ruiz, F. *Polyhedron* **2000**, 19, 1859.

[41] Tailor, S.M.; Patel, U.H. *J. Mol. Struct.* **2015**, 1088, 161.

[42] Singh, T.P.; Patel, U.H.; Haridas, M. *Acta Cryst.* **1984**, C40, 2088.

[43] Tailor, S.M.; Patel, U.H. *J. Coord. Chem.* **2015**, 68, 2192.

[44] Lin-Vien, D.; Colthup, N.B.; Fately, W.G.; Grasselli, J.G. The *Handbook of Infrared and Raman Characteristic Frequencies of Organic Molecules*, Academic Press, San Diego, **1991**.

[45] Nakamoto, K. *Infrared and Raman Spectra of Inorganic and Coordination Compounds*, John Wiley & Sons, USA, **1997**.

[46] Nakanishi, K. *IR-Absorption Spectroscopy – Practical*, Holden-Day Inc., San Francisco, **1962**.

[47] Macı´as, B.; Garcı´a, I.; Villa, M.V.; Borra´s, J.; Castin˜ eiras, A.; Sanz, F. *Polyhedron* **2002**, 21, 1229.

[48] Driessen, W.L.; van der Voort, P.H. *Inorg. Chim. Acta* **1977**, 21, 217.

[49] Adembri, G.; Speroni, G.; Califano, S. *Spectrochim. Acta* **1963**, 19, 1145.

[50] Simmons, W.W. *The Sadtler handbook of proton NMR spectra*, Sadtler Research Laboratories, Inc., **1978**.

[51] Cotton, F.A.; Wilkinson, G.; Murillo, C.A.; Bochmann, M. *Advanced Inorganic Chemistry*, sixth ed., Wiley-Interscience, New York, **1999**.

[52] Venugopala Reddy, K.R.; Keshavayya, J.; Seetharamappa, J. *Dyes Pigm.* **2003**, 59, 237.

[53] Broido, A. *J. Polymer Sci.* **1969**, 7, 1761.

[54] Coats, A.W.; Redfern, J.P. *Nature* **1964**, 201, 68.

[55] Vogel, T. *Textbook of practical organic chemistry*, fourth ed., John Wiley Inc., England, **1989**.

[56] Foye, W.O.; Lemke, T.L.; Williams, D.A. *Principles of Medicinal Chemistry*, fourth ed., MD: Williams & Wilkin, Baltimore, **1995**.

Table 1. Crystal data and refinement of $[Ni(C_{10}H_9N_4O_2S)_2(C_5H_5N)_2](C_5H_5N)(H_2O)_2$

Empirical formula	$C_{35}H_{37}N_{11}NiO_6S_2$
Formula weight	830.58
Crystal system	Monoclinic
Space group	$P2_1$
a (Å)	9.1861(2)
b (Å)	18.4188(4)
c (Å)	11.5883(2)
β (˚)	103.509(1)
Volume ($Å^3$)	1906.46(5)
Z	2
Temperature (K)	296.15
Crystal size (mm^3)	0.75× 0.51×0.42
Calculated density (Mg m^{-3}),	1.45
Absorption coefficient (mm^{-1})	0.679
F(000)	864
θ range for data collection (°)	1.8-27.5
Index ranges	$-11 \le h \le 7$; $-23 \le k \le 22$; $-7 \le l \le 15$
Reflections collected	16895
Unique reflections	8295
R_{int}	0.0212
Goodness-of-fit on F^2	1.065
Absorption correction	N.A.
Refinement method	Full Matrix Least Square of $\|F\|^2$
Data/parameters	8295/513
Final R indices [I≥2σ(I)]	R_1 = 0.036, wR_2 = 0.094
R indices (all data)	R_1 = 0.044, wR_2 = 0.099
Largest diff. peak and hole (e $Å^{-3}$)	0.41 and -0.26

Table 2. Fractional atomic coordinates and equivalent isotropic displacement parameters (Å^2)

Atom	x	y	z	Ueq (Å^2)
Ni	0.50922 (5)	0.37225 (4)	0.76209 (4)	0.03698 (12)
S1A	0.50437 (13)	0.23071 (6)	0.55788 (11)	0.0513 (3)
S1B	0.51578 (11)	0.51540 (5)	0.96293 (10)	0.0463 (3)
O1A	0.3964 (4)	0.2287 (2)	0.4453 (3)	0.0801 (11)
O1B	0.5530 (4)	0.55706 (18)	0.8695 (3)	0.0657 (9)
O2A	0.4731 (4)	0.1879 (2)	0.6540 (4)	0.0755 (10)
O2B	0.6210 (3)	0.5176 (2)	1.0765 (3)	0.0725 (10)
OWA	0.2100 (6)	0.1708 (3)	0.2480 (4)	0.133 (2)
OWB	0.7340 (6)	0.6116 (3)	1.2579 (5)	0.1250 (19)
N1	0.1428 (7)	0.3558 (5)	0.3106 (6)	0.116 (3)
N1A	0.5284 (4)	0.3113 (2)	0.6104 (3)	0.0430 (9)
N1B	0.4918 (4)	0.4349 (2)	0.9124 (3)	0.0391 (8)
N2A	0.5448 (4)	0.4311 (2)	0.6166 (3)	0.0429 (8)
N2B	0.4711 (4)	0.3151 (2)	0.9084 (3)	0.0398 (8)
N3A	0.5550 (3)	0.3730 (3)	0.4336 (2)	0.0513 (7)
N3B	0.4576 (3)	0.3741 (3)	1.0891 (2)	0.0488 (7)
N4A	1.0876 (5)	0.1288 (3)	0.4848 (5)	0.0834 (15)
N4B	−0.0876 (4)	0.6076 (3)	1.0038 (5)	0.0761 (13)
N5A	0.7400 (3)	0.3605 (2)	0.8323 (3)	0.0433 (8)
N5B	0.2776 (3)	0.3829 (2)	0.6917 (2)	0.0414 (8)
C1	0.0567 (7)	0.3069 (4)	0.2423 (5)	0.0811 (18)
C1A	0.6749 (5)	0.1987 (2)	0.5330 (3)	0.0469 (9)
C1B	0.3434 (4)	0.5476 (2)	0.9828 (3)	0.0435 (9)
C2	−0.0804 (8)	0.3272 (5)	0.1924 (6)	0.096 (2)
C2A	0.7133 (5)	0.2115 (3)	0.4270 (4)	0.0587 (12)
C2B	0.2516 (5)	0.5867 (3)	0.8915 (4)	0.0526 (10)
C3	−0.1370 (7)	0.3927 (5)	0.2097 (6)	0.092 (3)
C3A	0.8488 (6)	0.1881 (3)	0.4096 (4)	0.0642 (13)
C3B	0.1112 (5)	0.6080 (3)	0.9006 (4)	0.0582 (12)
C4	−0.0519 (8)	0.4406 (4)	0.2765 (7)	0.096 (2)
C4A	0.9500 (6)	0.1520 (3)	0.4997 (5)	0.0600 (12)
C4B	0.0569 (5)	0.5903 (3)	0.9992 (4)	0.0551 (11)
C5	0.0898 (8)	0.4239 (4)	0.3297 (7)	0.095 (2)
C5A	0.9074 (6)	0.1379 (3)	0.6046 (5)	0.0693 (14)
C5B	0.1535 (5)	0.5543 (3)	1.0925 (4)	0.0604 (12)
C6A	0.7719 (6)	0.1609 (3)	0.6214 (4)	0.0618 (12)
C6B	0.2949 (5)	0.5328 (3)	1.0837 (4)	0.0552 (11)
C7A	0.5436 (3)	0.3720 (3)	0.5462 (3)	0.0416 (7)
C7B	0.4728 (3)	0.3748 (3)	0.9768 (3)	0.0373 (7)

C8A	0.5554 (6)	0.4961 (3)	0.5685 (5)	0.0588 (12)
C8B	0.4575 (5)	0.2507 (3)	0.9582 (4)	0.0530 (11)
C9A	0.5655 (6)	0.5021 (3)	0.4514 (5)	0.0684 (14)
C9B	0.4435 (5)	0.2449 (3)	1.0736 (4)	0.0591 (11)
C10A	0.5647 (5)	0.4404 (3)	0.3898 (4)	0.0618 (13)
C10B	0.4421 (5)	0.3087 (3)	1.1339 (4)	0.0550 (11)
C11A	0.7986 (5)	0.2939 (3)	0.8505 (4)	0.0534 (11)
C11B	0.1856 (5)	0.3258 (3)	0.6620 (4)	0.0565 (12)
C12A	0.9493 (6)	0.2809 (3)	0.8944 (5)	0.0708 (14)
C12B	0.0345 (5)	0.3347 (4)	0.6152 (5)	0.0717 (17)
C13A	1.0419 (5)	0.3393 (4)	0.9222 (5)	0.0723 (16)
C13B	−0.0254 (6)	0.4016 (4)	0.5986 (5)	0.0779 (19)
C14A	0.9858 (6)	0.4074 (4)	0.9045 (5)	0.0744 (17)
C14B	0.0669 (5)	0.4611 (3)	0.6289 (5)	0.0701 (14)
C15A	0.8336 (5)	0.4151 (3)	0.8600 (4)	0.0565 (11)
C15B	0.2179 (5)	0.4488 (3)	0.6755 (4)	0.0533 (11)

Table 3. Selected bond lengths and angles for $[Ni(C_{10}H_9N_4O_2S)_2(C_5H_5N)_2](C_5H_5N)(H_2O)_2$

Bond distances (Å)		Bond angles (˚)	
Ni—N1A	2.128 (4)	N2A—Ni—N2B	178.84 (19)
Ni—N1B	2.126 (4)	N2A—Ni—N5A	91.83 (13)
Ni—N2A	2.093 (4)	N2B—Ni—N5A	88.82 (13)
Ni—N2B	2.094 (4)	N2A—Ni—N5B	88.46 (14)
Ni—N5A	2.097 (3)	N5A—Ni—N5B	179.45 (19)
Ni—N5B	2.102 (3)	N2A—Ni—N1B	115.74 (18)
S1A—O1A	1.444 (4)	N5A—Ni—N1B	90.04 (13)
S1A—O2A	1.447 (4)	N2A—Ni—N1A	63.23 (11)
S1A—N1A	1.599 (4)	N2B—Ni—N1A	117.74 (18)
S1A—C1A	1.759 (4)	N5A—Ni—N1A	89.70 (13)
N1A—C7A	1.369 (6)	N5B—Ni—N1A	90.02 (13)
N4A—C4A	1.383 (6)	N1B—Ni—N1A	178.93 (19)

Table 4. Hydrogen bond geometry and symmetry code for

$[Ni(C_{10}H_9N_4O_2S)_2(C_5H_5N)_2](C_5H_5N)(H_2O)_2$

D- H…A	D-H(Å)	H…A(Å)	D-A (Å)	∠D-H …A(°)
OWA—HWA2···O1A	0.95	1.81	2.733 (6)	163.9
OWB—HWB1···O2A^{i}	0.92	1.82	2.747 (6)	177.6
OWB—HWB2···N4A^{ii}	0.93	2.27	3.065 (7)	142.4
N4A—H4A1···OWB^{iii}	0.86	2.34	3.065 (7)	143
N4A—H4A2···OWA^{iv}	0.86	2.44	3.291 (7)	174
N4B—H4B1···OWA^{v}	0.86	2.3	3.098 (7)	153
C1—H1···OWA	0.93	1.97	2.869 (9)	163
C3B—H3B···OWA^{v}	0.93	2.47	3.260 (6)	143
C5A—H5A···OWB^{iii}	0.93	2.64	3.342 (7)	133
C9B—H9B···O1B^{vi}	0.93	2.65	3.520 (6)	157
C12A—H12A···N4B^{vi}	0.93	2.63	3.534 (8)	164
C14B—H14B···N4A^{vii}	0.93	2.63	3.524 (8)	161

Symmetry codes: (i) −x+1, y+1/2, −z+2; (ii) −x+2, y+1/2, −z+2; (iii) −x+2, y−1/2, −z+2; (iv) x+1, y, z; (v) −x, y+1/2, −z+1; (vi) −x+1, y−1/2, −z+2; (vii) −x+1, y+1/2, −z+1.

Table 5. Characteristic IR bands (cm^{-1}) of sulfadiazine and its nickel complex

Assignment	Sulfadiazine	Ni–sulfadiazine
N-H	3102	
$\nu_{as}(NH_2)$	3424	3450
$\nu_{s}(NH_2)$	3355	3360
$\delta(NH_2)$	1651	1628
ν-phenyl ring	1580, 1493	1595, 1558
$(SO_2)_{as}$	1325, 1262	1360, 1267
$(SO_2)_{sy}$	1156	1183
ν(S-N)	996, 942	1015, 989

Table 6. ^{1}H NMR shift assignments of sulfadiazine (1) and its nickel complex (2) in DMSO-d_6[a]

Assignment	^{1}H(1)	^{1}H(2)	Δδ(H)[b]
N(1A)–H	11.25	-	
C(8A)–H/C(10A) −H	8.48	8.30	-0.18
C(9A) −H	7.00	7.02	+0.02
C(2A)–H/C(6A) −H	7.62	7.43	-0.19
C(3A)–H/C(5A) −H	6.56	6.50	-0.06
NH_2	6.00	5.26	-0.74

[a]Relative to TMS with DMSO-d_6 peak as reference (^{1}H, 2.60 ppm)

[b]Δδ= δ(sulfonamide complex)- δ(sulfonamide).

Table 7. Absorbance, wavelength and assignment of sulfadiazine and its nickel complex

Ligand/ Complex	Wavelength (nm)	Energy (cm^{-1})	Assignment	Absorbance (A)
sdz	275	36363	$\pi \rightarrow \pi^*$ /n$\rightarrow\pi^*$overlap	2.1119
Ni-sdz	272	36764	$\pi \rightarrow \pi^*$	1.3316
	401	24937	$^3A_{2g} \rightarrow {}^3T_1g(F)$	0.8621
	625	16000	$^3A_{2g} \rightarrow {}^1E_g$	0.3076

Table 8. Thermodynamic parameters of sulfadiazine and its nickel complex

Ligand/ Complex	Decomposition Temperature range (K)	Activation Energy (kJ mol^{-1})	Arrhenius constant	ΔH (kJ mol^{-1})	ΔS (J K^{-1} mol^{-1})	ΔG (kJ mol^{-1})
sdz	528.80−568.80	148.85	31.27	144.28	-221.38	265.78
	592.80−632.80	28.42	5.58	23.33	-236.63	168.34
Ni-sdz	335.85−352.11	37.70	9.78	34.84	-227.15	112.94
	662.52−680.19	121.47	21.14	115.89	-226.31	267.84

Table 9. MIC value (µg/ml) of sulfadiazine and its nickel complex

Sulfa drug	MIC for *Escherichia coli* MTCC 442	MIC for *Staphylococcus aureus* MTCC 96
sdz	250	100
Ni-sdz	100	250
DMSO (control)	Nil	Nil

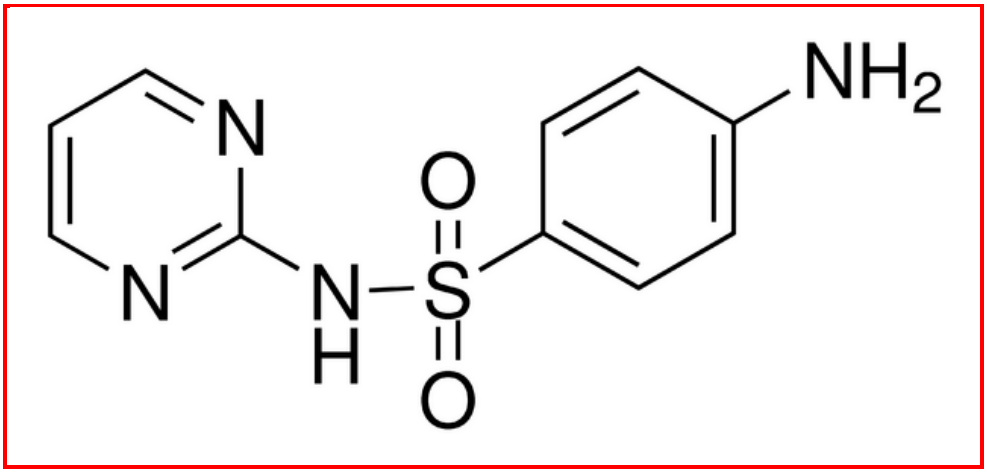

Figure 1. Chemical structure of sulfadiazine

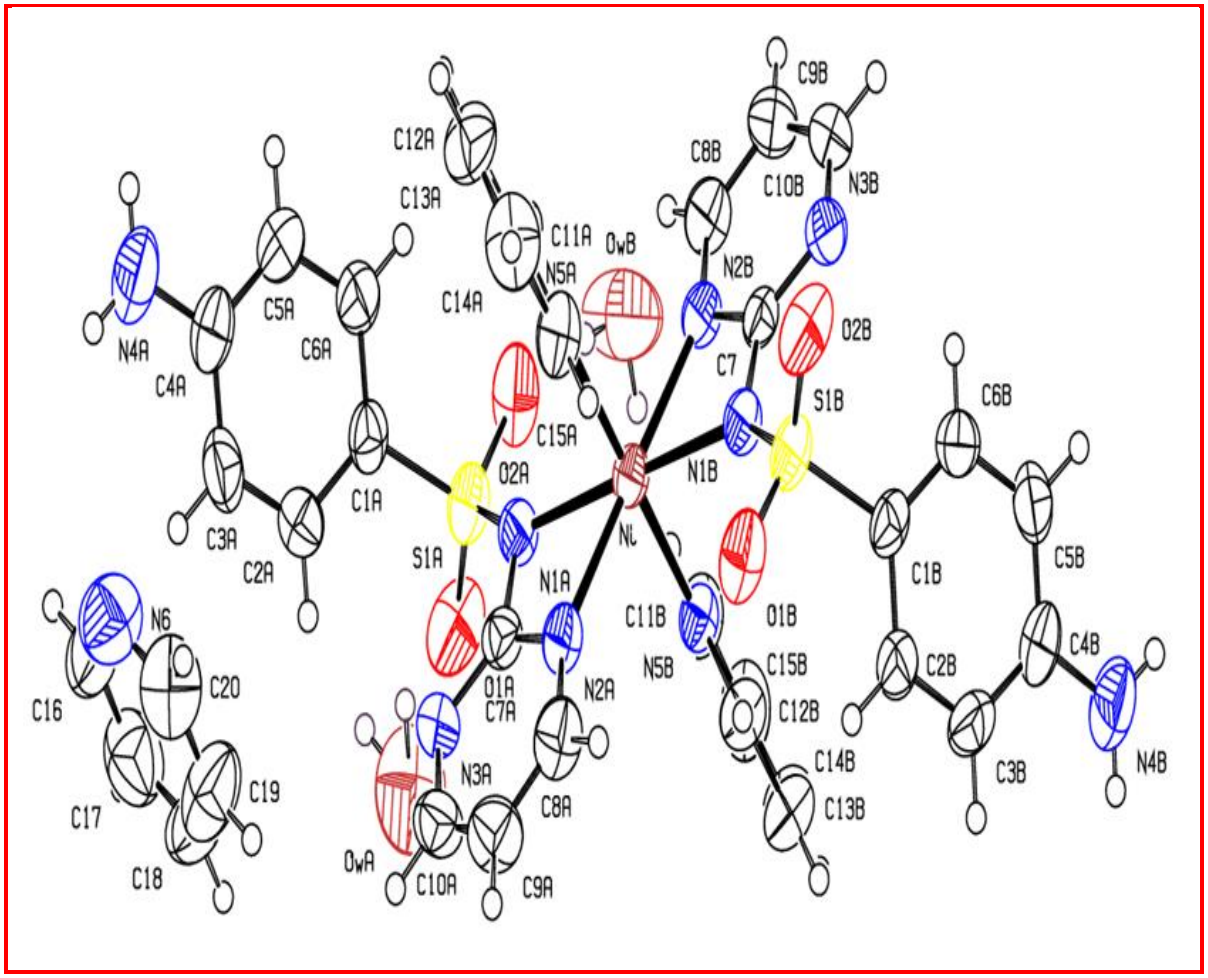

Figure 2. ORTEP diagram of the title compound with thermal displacement ellipsoids are drawn at 50% probability level

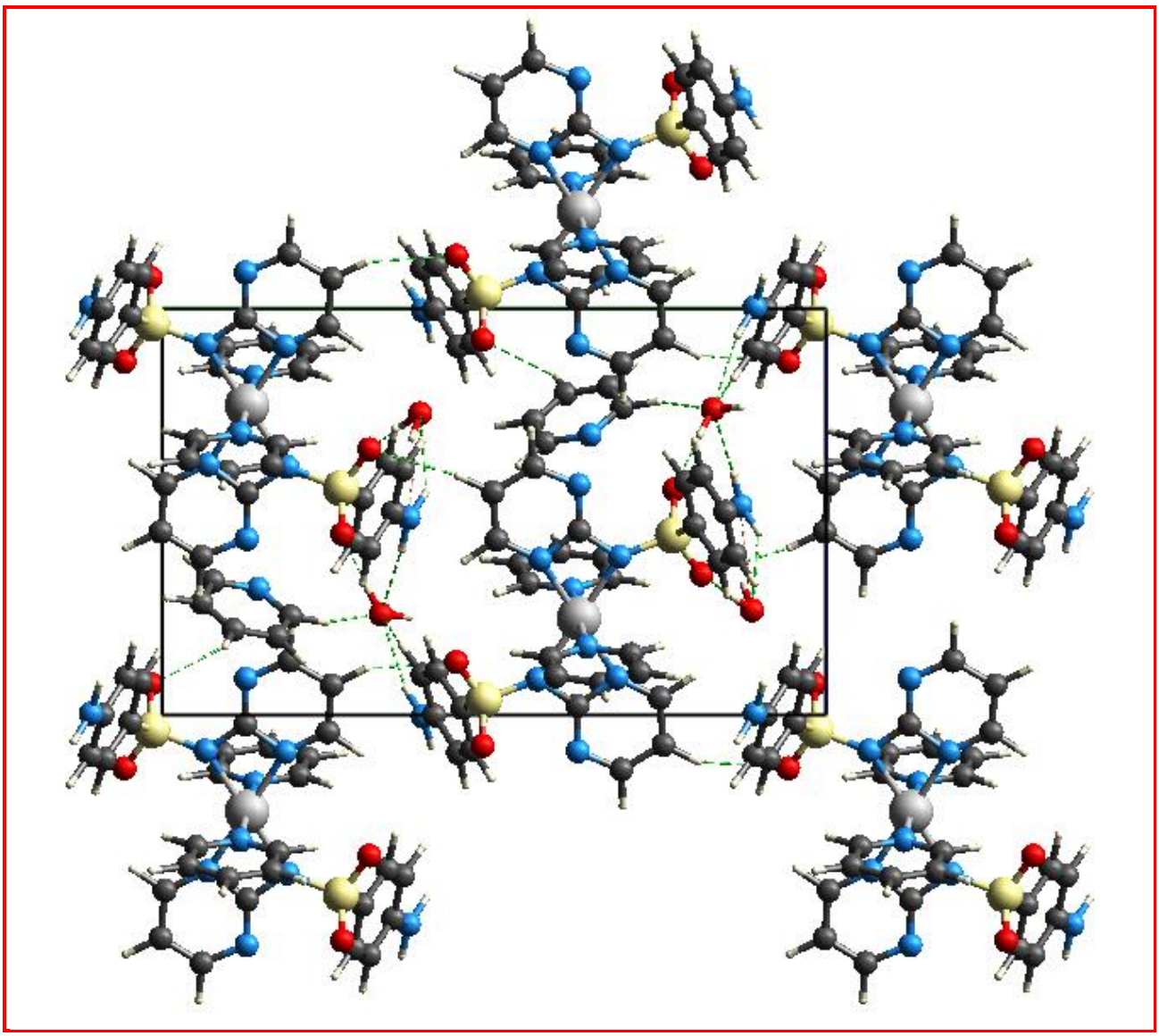

Figure 3. Molecular packing of title compound showing intermolecular N−H···O, O−H···O and C−H···O interactions

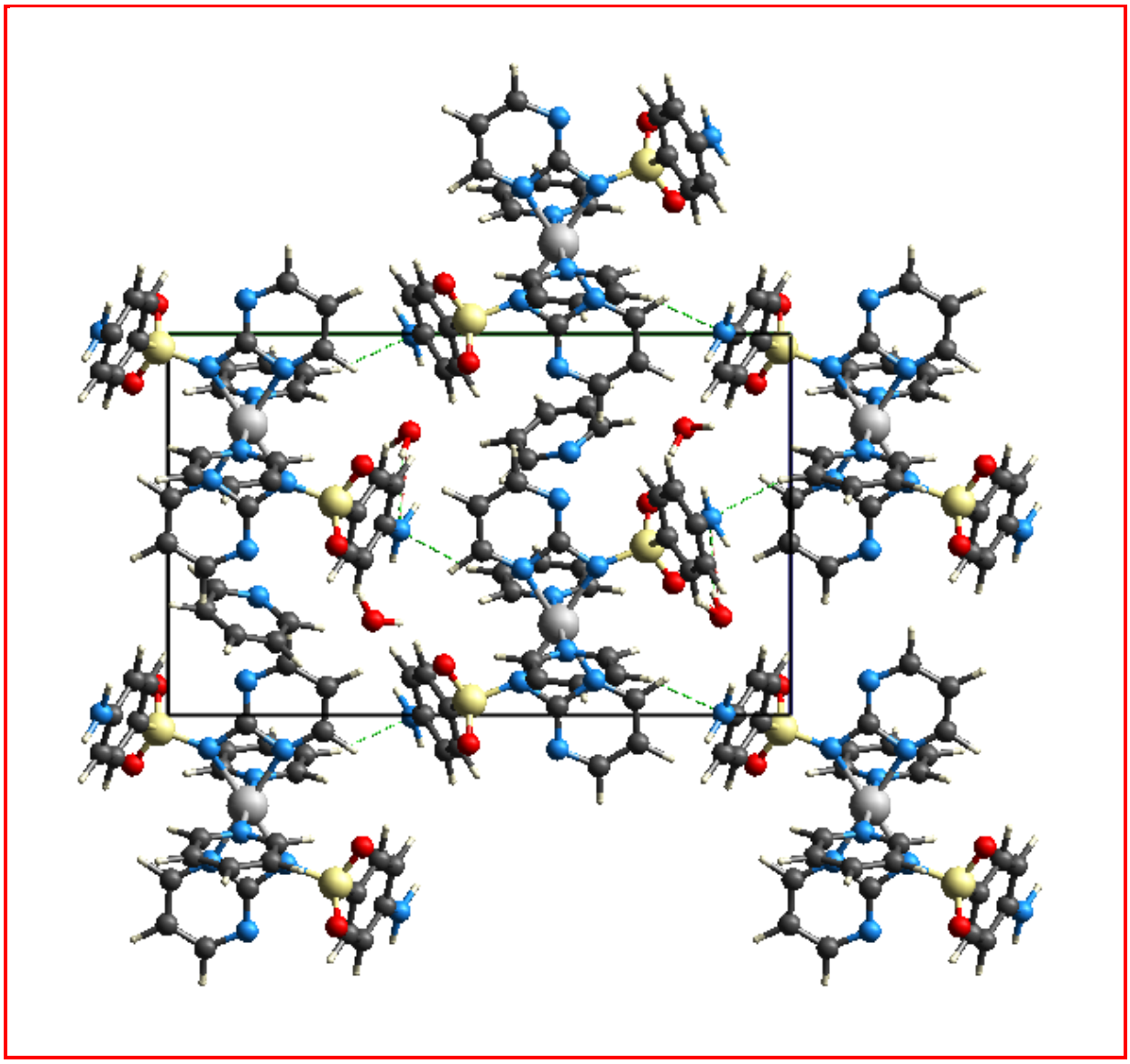

Figure 4. Molecular packing of title compound showing intermolecular C−H···N and O−H···N interactions

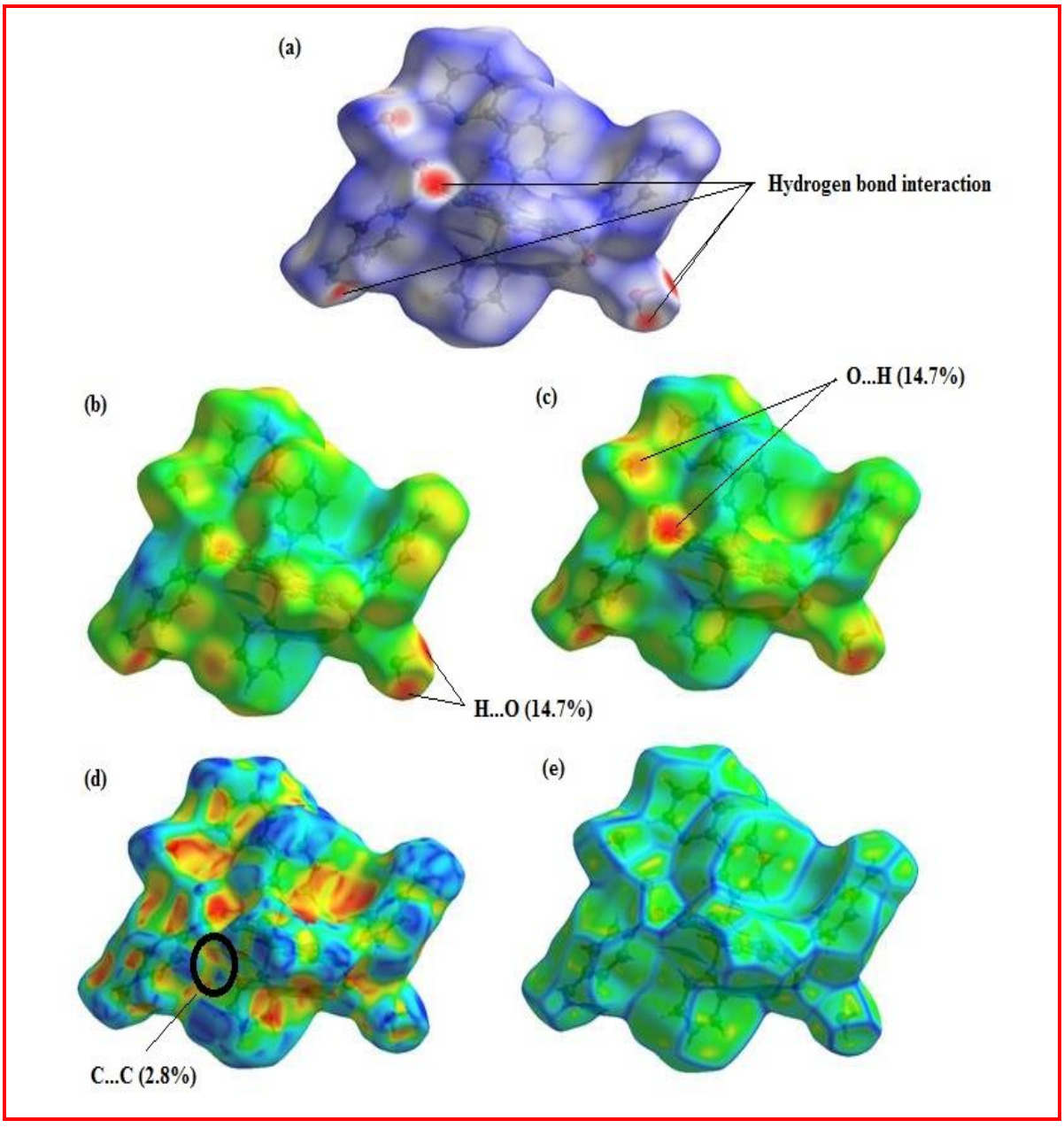

Figure 5. Hirshfeld surfaces mapped with (a) d_{norm}, (b) d_i, (c) d_e, (d) shape index and (e) curvedness of $[Ni(C_{10}H_9N_4O_2S)_2(C_5H_5N)_2](C_5H_5N)(H_2O)_2$

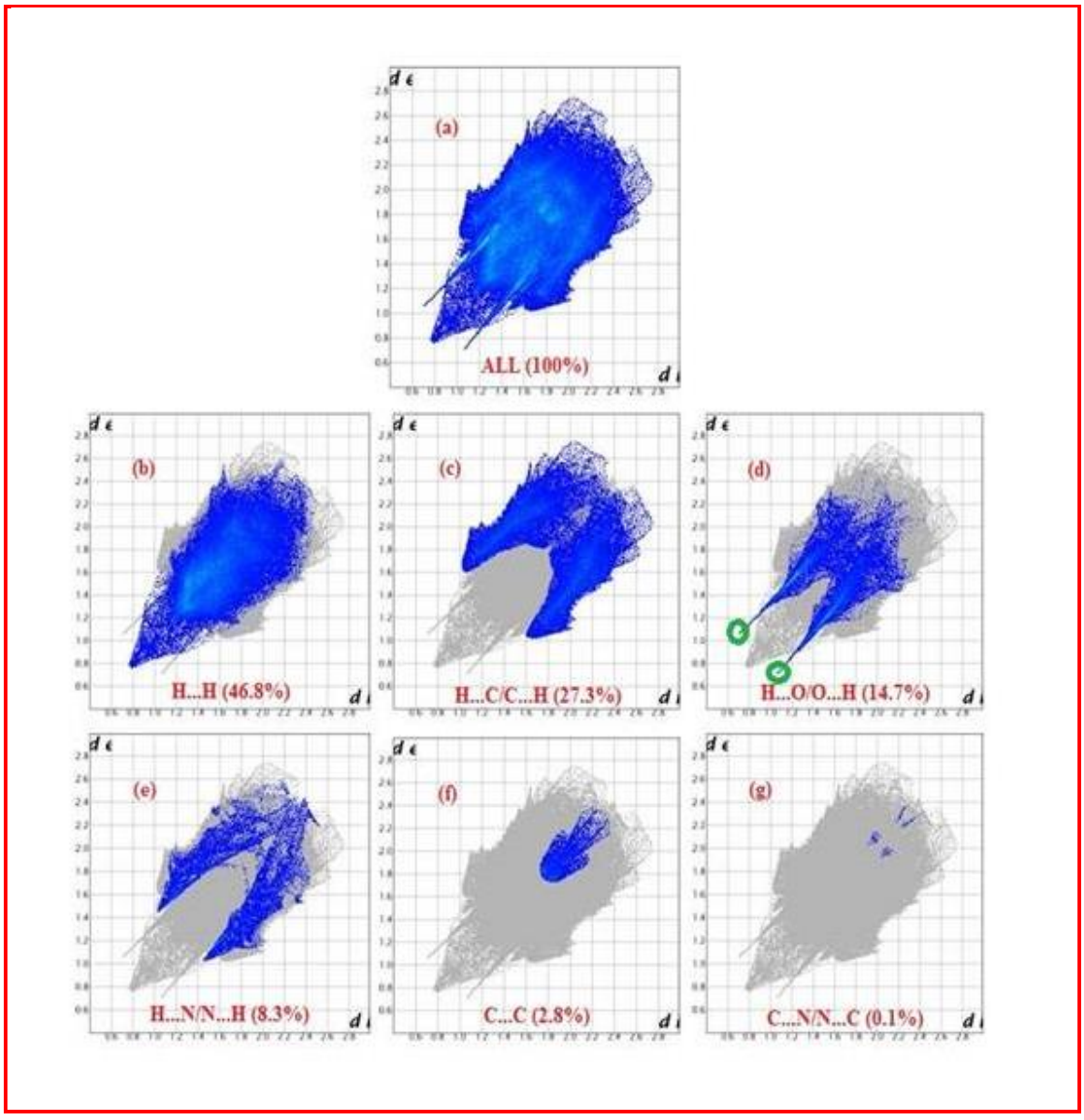

Figure 6. 2-D fingerprint plots of $[Ni(C_{10}H_9N_4O_2S)_2(C_5H_5N)_2](C_5H_5N)(H_2O)_2$: (a) full (b) resolved into H—H and (c) C—H (d) O—H (e) N—H (f) C—C (g) C—N contacts showing the percentages of contacts contributed to the total Hirshfeld surface area of molecule

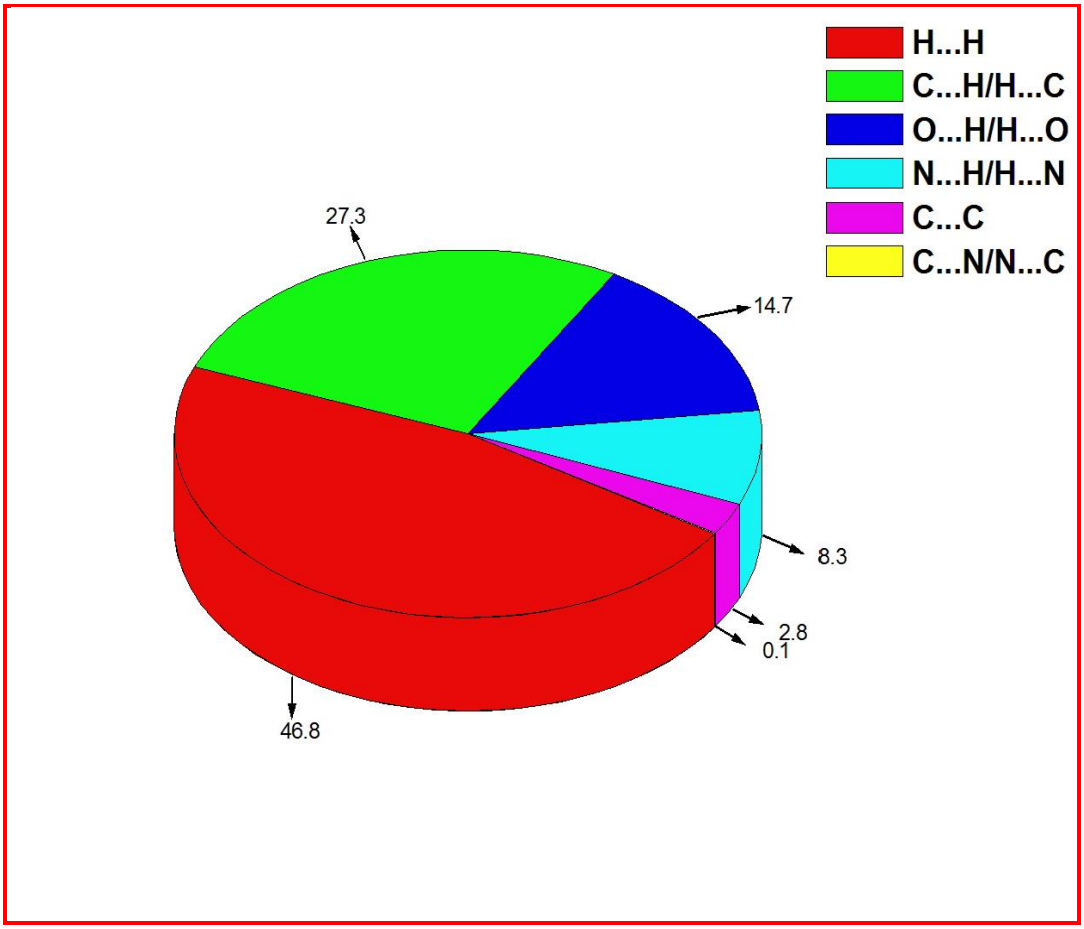

Figure 7. Relative contribution of various intermolecular interactions to the Hirshfeld surface area

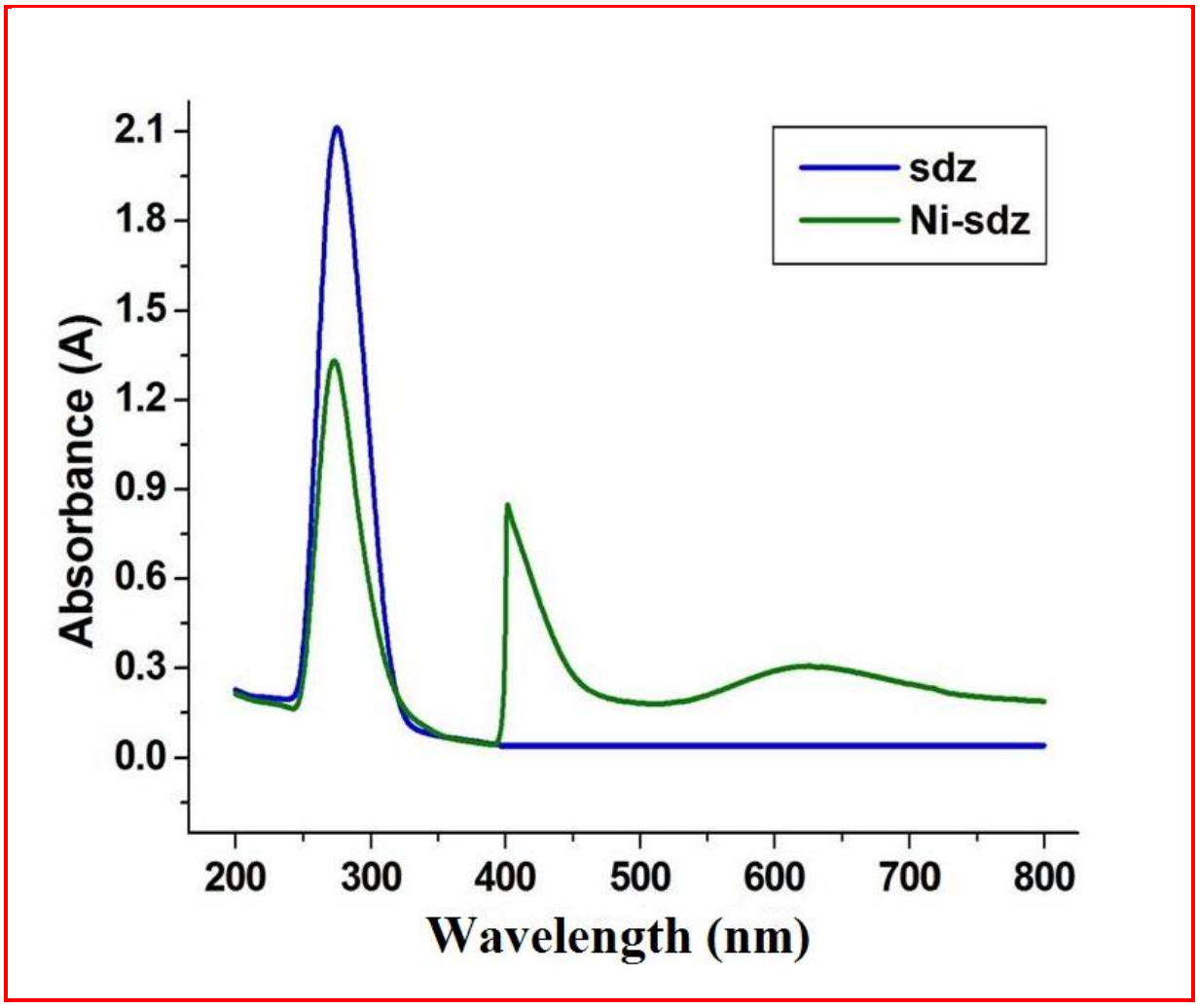

Figure 8. UV-Vis spectra

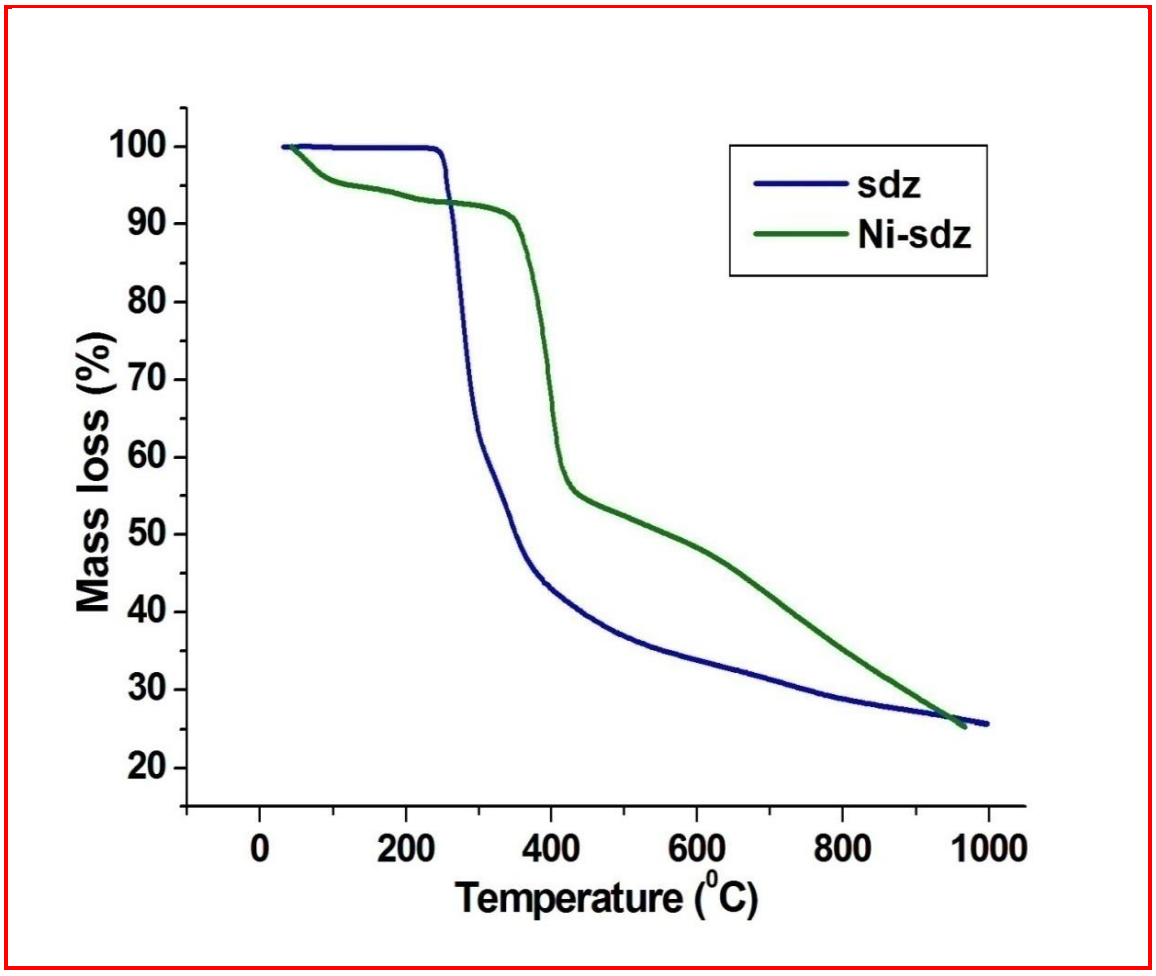

Figure 9. TGAcurve

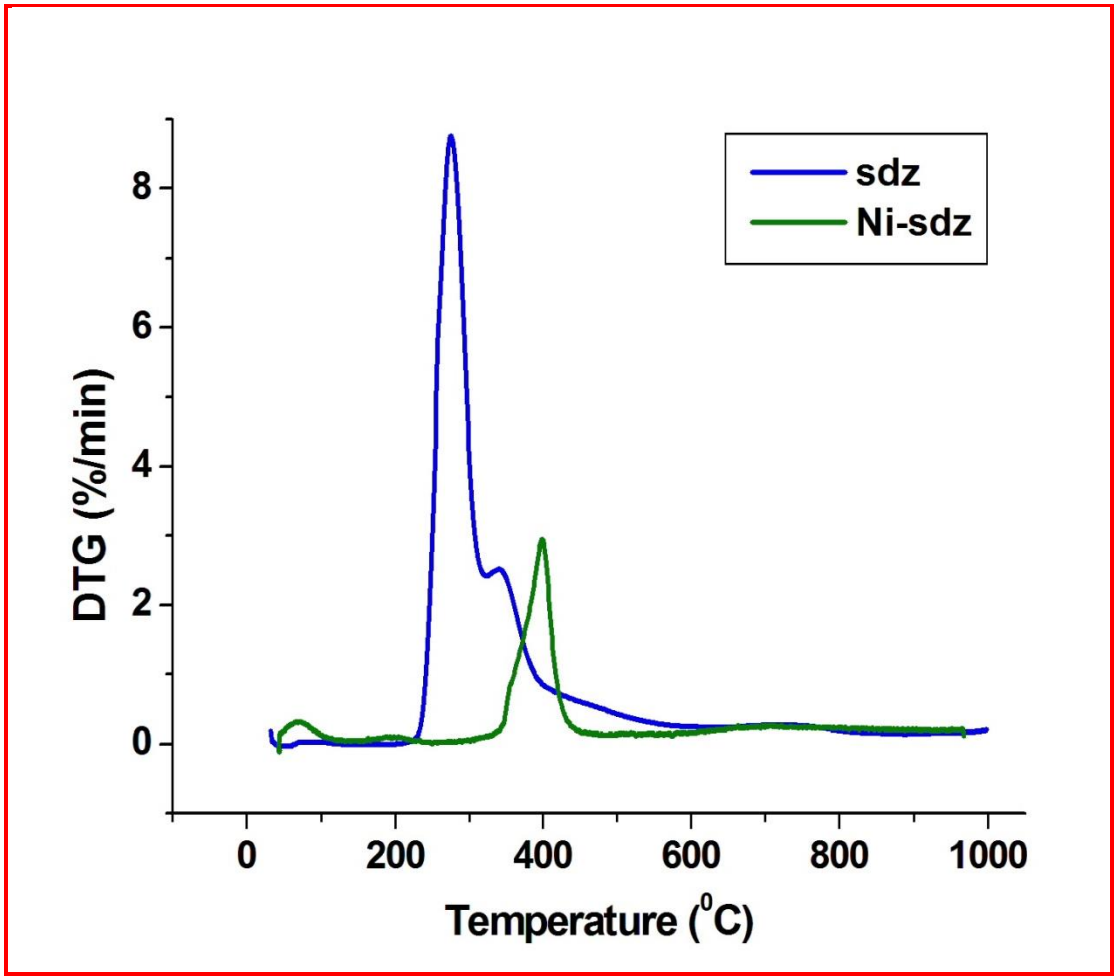

Figure 10. DTG curve

